

Robust H_∞ control applied on a fixed wing unmanned aerial vehicle

Caglar Uyulan*¹ and Mustafa Tolga Yavuz^{2a}

¹Department of Mechatronics Engineering, Bulent Ecevit University, Turkey

²Department of Aeronautics and Astronautics, Istanbul Technical University, Turkey

(Received August 3, 2018, Revised March 23, 2019, Accepted April 5, 2019)

Abstract. The implementation of a robust H_∞ Control, which is numerically efficient for uncertain nonlinear dynamics, on longitudinal and lateral autopilots is realised for a quarter scale Piper J3-Cub model accepted as an unmanned aerial vehicle (UAV) under the condition of sensor noise and disturbance effects. The stability and control coefficients of the UAV are evaluated through XFLR5 software, which utilises a vortex lattice method at a pre-defined flight condition. After that, the longitudinal trim point is computed, and the linearization process is performed at this trim point. The “ μ -Synthesis”-based robust H_∞ control algorithm for roll, pitch and yaw displacement autopilots are developed for both longitudinal and lateral linearised nonlinear dynamics. Controller performances, closed-loop frequency responses, nominal and perturbed system responses are obtained under the conditions of disturbance and sensor noise. The simulation results indicate that the proposed control scheme achieves robust performance and guarantees stability under exogenous disturbance and measurement noise effects and model uncertainty.

Keywords: aerodynamic; aeroplane equation of motion; flight control; nonlinear control; robust H_∞ control; multi-input multi-output control surface; μ -synthesis; unmanned aerial vehicles

1. Introduction

Nowadays UAVs are challenged to perform a wide mission spectrum efficient and accurate. Controlling UAVs is a competitive task since UAVs possess multi-input-multi-output (MIMO), underactuated, unstable and highly coupled system characteristics. Complete system dynamics information is necessitated to control this kind of nonlinear system. Since the system parameters are related with the operational conditions and subjected to the wear and tear effects, which leads to the parameter variance, UAVs carry parametric uncertainties, which drive the controller designed based on the nominal model to instability or performance degrade. There also exists a different kind of uncertain nonlinearity (such as nonlinear friction force, backlash, etc.), which is not able to be modelled accurately. Many control algorithms based on robust and adaptive control theory in the literature were proposed to handle uncertain nonlinear dynamics (Narendra *et al.* 1980, Ioannau and Sun 1991, Ioannau and Sun 1996, Ioannau and Datta 2006, Hassan and Rao

*Corresponding author, Ph.D., E-mail: caglaruyulan@beun.edu.tr

^aPh.D. Student, E-mail: yavuzmusta@itu.edu.tr

2005, Chang 2003, Wang *et al.* 2001, Buttler 1992, Aström and Wittenmark 2009, Guo *et al.* 2011, Tao and Joshi 2001, Ioannou and Kokotovic 1984, Tao 2003). The difference between a robust and adaptive controller can be stated that; a robust controller, which may utilise extreme actions to accomplish the goal, is designed to operate under the worst-case condition assumption. Oppositely, an adaptive controller conducts an online estimation of the process uncertainty and then produces a control input to predict, overcome or suppress the undesirable deviations from the preplanned closed-loop plant behaviour. Besides, these controllers can be designed to “learn” or equivalently to capture previously done events. For example, a tracking error integrator in a feedback loop, which accumulates and integrates regulation errors based on previous and current data, is a learning controller (Lavretsky and Wise 2013). As a result, the utilisation of robust and adaptive controllers is crucial in maintaining closed-loop stability, applying robustness to uncertainties and ensuring target performance. The lateral and longitudinal dynamics of aircraft has been controlled via robust H_∞ control method (Giacoman-Zarzar *et al.* 2008, Mystkowski 2013, Mystkowski 2014, Dorobantu *et al.* 2012).

In this paper, a robust H_∞ algorithm was constructed for both longitudinal and lateral linearized nonlinear dynamics of the fixed wing UAV via novel “ μ -Synthesis” methodology. Control and stability coefficients of the UAV were calculated using XFLR5 software implemented in MATLAB. Nonlinear equations of motion (EOM) were obtained using Newton's second law and kinematic relations. These nonlinear EOM were constructed in Simulink and then solved with the 4th order Runge-Kutta method. Longitudinal trim point of the UAV was evaluated through the Gauss-Seidel iteration method at a given flight condition. After that, the linearization process was conducted at the calculated trim point. Roll, pitch and yaw displacement autopilots were built based on the root locus method and utilized as reference models for performance evaluation. Afterwards, robust autopilots were designed and simulated in SIMULINK considering disturbance and measurement noise effects. According to the results of the controller performances, closed-loop frequency responses, nominal and perturbed system responses, it can be deduced that the “ μ -Synthesis” methodology is a quite good solution for controlling UAV dynamics under the aforementioned conditions.

2. Mathematical model of the UAV

Before controlling UAV, a satisfactory mathematical model must be derived by stating UAV geometric parameters, flight conditions and EOM, respectively. Therefore, a linearised mathematical model of the quarter scale Piper J3-Cub were constructed from its stability coefficients. To alter the aircraft body into a determined state from its current state, the external moments and forces should be applied. An aircraft control surface produces the external force or moment exerting to the aircraft body. The force or moment occurrence mechanism related with the aerodynamics law can be described as the movement of the control surface on its hinge axis when a pilot or control system transmits a command signal to the control surface. Pulse width modulation (PWM) controlled R/C servo motors are the actuator of the control surfaces. In the conventional aircraft, three primary control surfaces are named as “aileron, rudder and elevator”. While aileron generates moment on the x -axis, elevator and rudder produce moments on y and z -axis, respectively. Aileron is responsible from roll motion, elevator and rudder control pitch and yaw motion, respectively (McLean 1990). The 6-DOF motion of an aerial vehicle is decomposed into a steady-state motion. The perturbation dynamics are captured near an operating point by

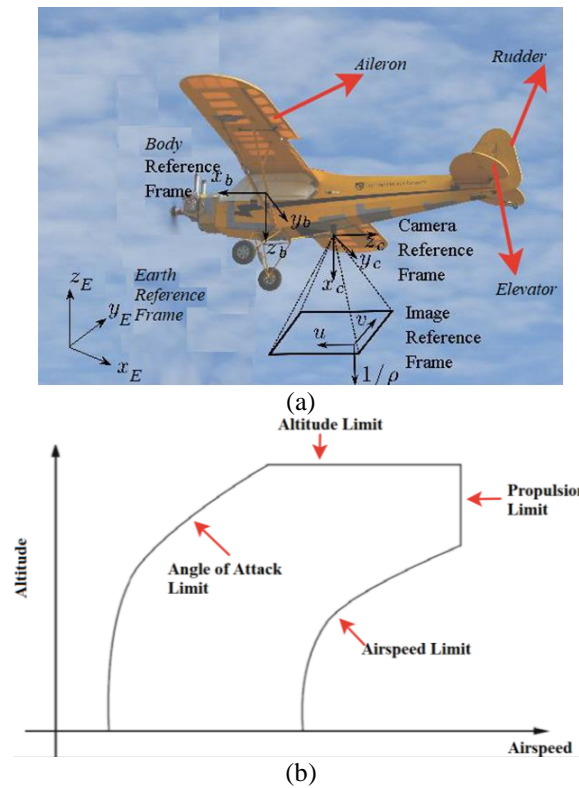


Fig. 1 (a) The picture of the Piper J3-Cub with reference frame and control surfaces (Abuhashim and Sukkarieh 2012) and (b) Aircraft operational flight envelope as a function of altitude and air-speed (Lavretsky 2013)

Table 1 Geometric specifications of the UAV and flight initial conditions (Du 2011)

Geometric Specifications of the UAV				Initial Conditions of the Flight	
Wing Span	2680,5 mm	Ix	0,9036 kgm ²	Cruise Speed	15 $\frac{m}{s}$
Wing Chord	400 mm	Iy	0,8196 kgm ²	Altitude	150 m
Fuselage Length	1727 mm	Iz	1,4721 kgm ²	Air Density	1,2075 $\frac{kg}{m^3}$
Weight	5,5 kg	Ixz	0,0648 kgm ²	Initial Angle of Attack	0°
Wing Area	1,02 m ²	Ixy	0 kgm ²	Initial Angle of Sideslip	0°
Wing Profile	USA35 – B	Iyz	0 kgm ²	Initial Roll Angle	0°
Center of Gravity-x	-500 mm	Center of Gravity-z	12 mm	Initial Pitch Angle	0°
Center of Gravity-y	0 mm			Initial Yaw Angle	0°

conducting a trimming process, which means to finding a balance or equilibrium among aerodynamic, propulsive and gravitational forces and moments acting on the UAV. A reduced

Table 2 Stability and control derivatives of the UAV

Stability Derivatives											
Derivatives of Lift Coefficient		Derivatives of Drag Coefficient		Derivatives of Side Force Coefficient		Roll Derivatives		Pitch Derivatives		Yaw Derivatives	
C_{L_α}	5,0996	C_{D_α}	0,1745	C_{y_α}	0	C_{l_α}	0	C_{m_α}	-2,5927	C_{n_α}	0
C_{L_β}	0	C_{D_β}	0	C_{y_β}	-0,2067	C_{l_β}	-0,010605	C_{m_β}	0	C_{n_β}	0,1071
C_{L_p}	0	C_{D_p}	0	C_{y_p}	-0,00815	C_{l_p}	-0,51261	C_{m_p}	0	C_{n_p}	-0,0276
C_{L_q}	8,4994	C_{D_q}	0,1885	C_{y_q}	0	C_{l_q}	0	C_{m_q}	-17,212	C_{n_q}	0
C_{L_r}	0	C_{D_r}	0	C_{y_r}	0,2179	C_{l_r}	0,047953	C_{m_r}	0	C_{n_r}	-0,1219
Control Derivatives						Unsteady Derivatives					
Elevator		Aileron		Rudder							
$C_{L_{\delta_e}}$	0,4528	$C_{y_{\delta_a}}$	-0,007426	$C_{y_{\delta_r}}$	0,15505	$C_{m_{\dot{\alpha}}}$	-5,982	$C_{y_{\dot{\beta}}}$	-0,078		
$C_{D_{\delta_e}}$	0	$C_{l_{\delta_a}}$	0,3318	$C_{l_{\delta_r}}$	0,002908	$C_{n_{\dot{\alpha}}}$	-2,976	$C_{n_{\dot{\beta}}}$	-0,292		
$C_{m_{\delta_e}}$	-1,646	$C_{n_{\delta_a}}$	-0,015714	$C_{n_{\delta_r}}$	-0,08853						

tractable form of the nonlinear fully coupled 6-DOF aircraft dynamics obtained by utilizing such a decomposition is suitable for control design and analysis purposes. An aircraft is trimmed by adjusting its primary controls to values that would satisfy the desired steady-state flight conditions (Lavretsky 2014). From mathematical terms, it is derived that a system has an equilibrium pair $(\vec{x}_{eq}, \vec{u}_{eq})$ in $\dot{\underline{x}} = f(\underline{x}, \underline{u})$, $\underline{y} = h(\underline{x}, \underline{u})$ such that the translational and angular accelerations take the value of zero (Khalil 2015, Valavanis 2015).

$$\mathbf{0} = f(\vec{x}_{eq}, \vec{u}_{eq})$$

Accelerated flight equilibrium or steady-state flight conditions should be determined before constructing the mathematical model. The picture of the Piper J3-Cub with the coordinates and control surfaces was demonstrated in Fig. 1(a). An aircraft operates at the multiple distinct equilibrium points throughout the UAV flight operational envelope as depicted in Fig. 1(b).

The longitudinal and lateral-directional modes, which are necessitated to analyse system equations, are obtained after decomposing the aircraft dynamics by trimming at flight conditions. The force equations in x and z directions and pitching moment equations comprise the longitudinal mode. The lateral mode consists of the force equation in y direction, rolling and yawing moment equations. The detailed procedure of deriving these two kinds of equation systems is represented in APPENDIX-I. The applied forces and moments acting on the UAV comprise gravitational, aerodynamic and the thrust part, respectively.

The aerodynamic forces and moments are given in APPENDIX-II. Nonlinear EOMs were structured based on Newton's second law and kinematic relationships after calculating the coefficients and moments of inertias. It can be observed that there exist three longitudinal dynamical, three lateral dynamical, three kinematic and three coordinate equations. These nonlinear equations are solved through fourth order Runge-Kutta method in SIMULINK. Geometric specification and flight conditions of a quarter scale Piper J3-Cub are tabulated in Table 1.

Table 3 UAV trim point

UAV trim point for $U_0 = 15 \frac{m}{s}, h = 150 m, m = 5,5 kg$	
Trimmed δ_T	0,0143
Trimmed δ_e	0,0165°
Trimmed α	-0,1314°
Lift Force	53,9158 N
Drag Force	2,6877 N
Thrust Force	2,6902 N
Pitching Moment Coefficient	0,0015
Pitching Moment	0,0878 N

2.1 Stability and control derivatives

The stability coefficients of the quarter scale Piper J3-Cub are calculated through the help of XFLR5 program. The XFLR5 is software which could evaluate the stability coefficients by applying 3-D vortex lattices method. Wings, ailerons, horizontal stabiliser, elevator, vertical stabiliser and rudder geometries are sketched. After creating the geometry, trim conditions are specified. Analysis results are presented in Table

2.2 Calculation of the trim conditions

The pitching moment must be equal to zero ($C_m = 0$) to provide the longitudinal trim condition of a UAV in cruising flight. For a steady state horizontal flight, the following assumptions must be taken into consideration.

$$\theta = \alpha$$

$$\dot{u}, \dot{w}, \dot{q}, p, r, \phi = 0$$

Eq. (1)-(3) can be obtained by substituting aerodynamic force and moment equations in the APPENDIX-II into the longitudinal motion equations, which are given in APPENDIX-I.

$$0 = mg \sin(\alpha) - (C_{D_0} + C_{D_\alpha} \alpha + C_{D_{\delta_e}} \delta_e) Q S \cos(\alpha) + (C_{L_0} + C_{L_\alpha} \alpha + C_{L_{\delta_e}} \delta_e) Q S \sin(\alpha) + T_{\max} \delta_T \cos(\phi_T) \quad (1)$$

$$0 = mg \cos(\alpha) - (C_{D_0} + C_{D_\alpha} \alpha + C_{D_{\delta_e}} \delta_e) Q S \sin(\alpha) - (C_{L_0} + C_{L_\alpha} \alpha + C_{L_{\delta_e}} \delta_e) Q S \cos(\alpha) + T_{\max} \delta_T \sin(\phi_T) \quad (2)$$

$$0 = (C_{m_0} + C_{m_\alpha} \alpha + C_{m_{\delta_e}} \delta_e) Q S c - T_{\max} \delta_T z_T \quad (3)$$

These equations correspond to x -force, z -force and pitching moment equation, respectively. δ_T , α , δ_e are acquired from Eq.(1)-Eq.(3) and solved by using the Gauss-Seidel method. The results are presented in the Table 3.

The comparison of the aircraft mass vs lift force and drag force vs thrust force should be made for a longitudinal trim point. The mass of the aircraft must be equal to the lift force, and the drag force must be equal to the thrust force to achieve a trim point. Also, the pitching moment coefficient is almost zero. As a conclusion of the trimming analysis, the linearization can be

performed at this trim point.

2.3 Linearization of the nonlinear EOMs at the trim conditions

At the calculated trim point, sufficient forces and moments are stated to sustain longitudinal stability. The stability and control derivatives, which are presented in Table 2, are utilised for $15 \frac{m}{s}$ forward velocity, 150 m altitude, 5,5 kg UAV mass and nearly zero angle of attack and sideslip angle. The nonlinear equations developed are linearized and simplified by using small-disturbance theory.

In applying small-disturbance theory, it can be assumed that the motion of the aeroplane consists of small deviations about a steady flight condition. This theory cannot be applied to problems in which large-amplitude motions are to be expected (e.g. spinning or stalled flight). Reference value plus a perturbation replaces all the variables in nonlinear equations. The propulsive force remains constant, and the reference flight condition is symmetric. The aerodynamic forces and moments are expressed as a function of all motion variables. The linearised EOM for longitudinal and lateral modes are presented in the following expressions.

Longitudinal EOM

$$\left(\frac{d}{dt} - X_u\right)\Delta u - X_w\Delta w + g\cos(\theta_0)\Delta\theta = X_{\delta_e}\Delta\delta_e + X_{\delta_T}\Delta\delta_T \quad (4)$$

$$-Z_u\Delta u + [(1 - Z_{\dot{w}})\frac{d}{dt} - Z_w]\Delta w - [(U_0 + Z_q)\frac{d}{dt} - g\sin(\theta_0)]\Delta\theta = Z_{\delta_e}\Delta\delta_e + Z_{\delta_T}\Delta\delta_T \quad (5)$$

$$-M_u\Delta u - (M_{\dot{w}}\frac{d}{dt} + M_w)\Delta w + \left(\frac{d^2}{dt^2} - M_q\frac{d}{dt}\right)\Delta\theta = M_{\delta_e}\Delta\delta_e + M_{\delta_T}\Delta\delta_T \quad (6)$$

Lateral EOM

$$\left(\frac{d}{dt} - Y_v\right)\Delta v - Y_p\Delta p + (u_0 - Y_r)\Delta r - g\cos(\theta_0)\Delta\phi = Y_{\delta_r}\Delta\delta_r \quad (7)$$

$$-L_v\Delta v + \left(\frac{d}{dt} - L_p\right)\Delta p - \left(\frac{I_{xz}}{I_x}\frac{d}{dt} + L_r\right)\Delta r = L_{\delta_a}\Delta\delta_a + L_{\delta_r}\Delta\delta_r \quad (8)$$

$$-N_v\Delta v - \left(\frac{I_{xz}}{I_z}\frac{d}{dt} + N_p\right)\Delta p + \left(\frac{d}{dt} - N_r\right)\Delta r = N_{\delta_a}\Delta\delta_a + N_{\delta_r}\Delta\delta_r \quad (9)$$

In conclusion, longitudinal and lateral stability parameters (derivatives) are shown in APPENDIX-III.

2.4 Linear longitudinal model

The longitudinal dynamics of the UAV is composed of forward, vertical and pitching motions, which are decomposed into fast (short-period) and slow (phugoid) modes. The main distinction between these modes is the time-scale separation. In the short-period mode, there exists a quick coupling among the angle of attack and pitch rate. The phugoid mode demonstrates a relatively slower dynamic interchange between the altitude and airspeed. These modes are emerged after linearising the UAV model around an equilibrium point (trim point). It is assumed that the thrust line is aligned with the x -axis of the UAV (Nelson 1998).

Rewriting the Eq.(4)-Eq.(6) in the state-space form ($\dot{\underline{x}} = A_{\text{long}}\underline{x} + B_{\text{long}}\underline{u}$; $\underline{y} = C_{\text{long}}\underline{x} + D_{\text{long}}\underline{u}$) yields

$$\begin{bmatrix} \Delta \dot{u} \\ \Delta \dot{w} \\ \Delta \dot{q} \\ \Delta \dot{\theta} \end{bmatrix} = \begin{bmatrix} X_u & X_w & 0 & -g \\ Z_u & Z_w & U_0 & 0 \\ M_u + M_{\dot{w}}Z_u & M_w + M_{\dot{w}}Z_w & M_q + M_{\dot{w}}U_0 & 0 \\ 0 & 0 & 1 & 0 \end{bmatrix} \begin{bmatrix} \Delta u \\ \Delta w \\ \Delta q \\ \Delta \theta \end{bmatrix} + \begin{bmatrix} X_{\delta_e} & X_{\delta_r} \\ Z_{\delta_e} & Z_{\delta_r} \\ M_{\delta_e} + M_{\dot{w}}Z_{\delta_e} & M_{\delta_r} + M_{\dot{w}}Z_{\delta_r} \\ 0 & 0 \end{bmatrix} \begin{bmatrix} \delta_e \\ \delta_r \end{bmatrix} \quad (10)$$

The force derivatives of Z_q and $Z_{\dot{w}}$ are usually not contribute to the aircraft response. Therefore, these parameters are neglected to simplify the representation of the EOM in the state-space form. Linear longitudinal state-space matrices are obtained by calculating the values in APPENDIX-III as follows

$$A_{\text{long}} = \begin{bmatrix} -0.06729 & 1.052 & 0 & -9.806 \\ -1.346 & -8.613 & 15 & 0 \\ 0.4848 & -8.606 & -20.95 & 0 \\ 0 & 0 & 1 & 0 \end{bmatrix} \quad B_{\text{long}} = \begin{bmatrix} 0 & 3.6 \\ -11.43 & 0 \\ -107.5 & 0 \\ 0 & 0 \end{bmatrix}$$

$$C_{\text{long}} = \begin{bmatrix} 1 & 0 & 0 & 0 \\ 0 & 1 & 0 & 0 \\ 0 & 0 & 1 & 0 \\ 0 & 0 & 0 & 1 \end{bmatrix} \quad D_{\text{long}} = \begin{bmatrix} 0 & 0 \\ 0 & 0 \\ 0 & 0 \\ 0 & 0 \end{bmatrix}$$

The matrix components in Eq.(10) represent constant stability and control derivatives of the UAV forces and moments concerning the longitudinal states and control inputs for a fixed flight condition. If the specific UAV parameter values of these derivatives are substituted into this model, most of the open-loop system eigenvalues are composed of a fast (short period) and slow (long period) pair of complex conjugate numbers. The time-scale separation in the longitudinal dynamics is derived through the help of this kind of decomposition.

Long period (Phugoid) mode

Deviations in pitch attitude, altitude and forward velocity take place at a nearly constant angle of attack and pitching moment equation is neglected in the long period (phugoid) mode ($\Delta\alpha \rightarrow 0, \Delta w \rightarrow 0$) (Nelson 1998). The damping of this mode is affected by the ratio of the drag to the lift. The lift force is constant and equal to the weight of the UAV in a straight flight. Therefore, it can be derived that the damping ratio of the phugoid mode is proportional to the total drag force. If the speed of the UAV increases, the total drag force and phugoid mode damping ratio will increase too. At the same time, when the altitude at constant speed is getting higher, the phugoid mode damping ratio decreases due to the decrease in drag force, which arises from the lower air density at higher altitude. The long period oscillations are not represented in this mode because they are quite small compared to the magnitude of oscillations obtained from the linear longitudinal model. Thus, the phugoid mode approximation is not satisfactory for simulation and control purposes (Blakelock 1991).

Short period mode

After assuming $\Delta u = 0$, dropping the x-force equation and considering $\Delta\alpha = \frac{\Delta w}{U_0}$, the state-space representation in Eq.(10) is transformed as the following expression

$$\begin{bmatrix} \Delta \dot{\alpha} \\ \Delta \dot{q} \\ \Delta \dot{\theta} \end{bmatrix} = \begin{bmatrix} \frac{Z_\alpha}{U_0} & 1 & 0 \\ M_\alpha + M_\alpha \frac{Z_\alpha}{U_0} & M_q + M_\alpha & 0 \\ 0 & 1 & 0 \end{bmatrix} \begin{bmatrix} \Delta\alpha \\ \Delta q \\ \Delta\theta \end{bmatrix} + \begin{bmatrix} \frac{Z_{\delta_e}}{U_0} \\ M_{\delta_e} + \frac{M_{\dot{\alpha}}}{U_0} Z_{\delta_e} \\ 0 \end{bmatrix} \delta_e \quad (11)$$

The linear longitudinal state-space matrices in short period mode are evaluated as follows

$$A_{\text{longsp}} = \begin{bmatrix} -8.613 & 1 & 0 \\ -129.1 & -20.95 & 0 \\ 0 & 1 & 0 \end{bmatrix} \quad B_{\text{longsp}} = \begin{bmatrix} -0.762 \\ -107.5 \\ 0 \end{bmatrix}$$

$$C_{\text{longsp}} = \begin{bmatrix} 1 & 0 & 0 \\ 0 & 1 & 0 \\ 0 & 0 & 1 \end{bmatrix} \quad D_{\text{longsp}} = \begin{bmatrix} 0 \\ 0 \\ 0 \end{bmatrix}$$

The dynamics of the UAV due to an elevator input are described using Eq.(11) on a short interval of time. The short-period system is suitable to develop robust and adaptive control methods for longitudinal autopilots. The natural frequency of the short period mode oscillation is proportional to the forward speed while damping ratio and altitude are constant. The damping ratio and natural frequency of the oscillation are proportional to $\sqrt{\rho}$ (inversely proportional to altitude). The oscillation frequency and damping ratio are quite significant in short period motion analysis (Blakelock 1991).

2.5 Linear lateral model

The lateral dynamics of the UAV are derived by linearization of the 6-DOF system around a selected trim point assuming constant thrust, airspeed, and angle of attack. The lateral-directional EOM consist of the side force, rolling and yawing dynamics described in Eq.(7)-Eq.(9), which can be rearranged into the state-space form as the following expression

$$\begin{bmatrix} \Delta \dot{v} \\ \Delta \dot{p} \\ \Delta \dot{r} \\ \Delta \dot{\phi} \end{bmatrix} = \begin{bmatrix} Y_v & Y_p & -(u_0 - Y_r) & g \cos \theta_0 \\ L_v & L_p & L_r & 0 \\ N_v & N_p & N_r & 0 \\ 0 & 1 & 0 & 0 \end{bmatrix} \begin{bmatrix} \Delta v \\ \Delta p \\ \Delta r \\ \Delta \phi \end{bmatrix} + \begin{bmatrix} 0 & Y_{\delta_r} \\ L_{\delta_a} & L_{\delta_r} \\ N_{\delta_a} & N_{\delta_r} \\ 0 & 0 \end{bmatrix} \begin{bmatrix} \delta_a \\ \delta_r \end{bmatrix} \quad (12)$$

It is sometimes convenient to use the sideslip angle instead of the side velocity. These two quantities are related to each other in the following way

$$\Delta \beta \simeq \tan^{-1} \left(\frac{\Delta v}{U_0} \right)$$

Using the above relationship, Eq.(12) can be expressed regarding the sideslip angle as Eq. (13)

$$\begin{bmatrix} \Delta \dot{\beta} \\ \Delta \dot{p} \\ \Delta \dot{r} \\ \Delta \dot{\phi} \end{bmatrix} = \begin{bmatrix} \frac{Y_\beta}{U_0} & \frac{Y_p}{U_0} & -(1 - \frac{Y_r}{U_0}) & \frac{g \cos \theta_0}{U_0} \\ L_\beta & L_p & L_r & 0 \\ N_\beta & N_p & N_r & 0 \\ 0 & 1 & 0 & 0 \end{bmatrix} \begin{bmatrix} \Delta \beta \\ \Delta p \\ \Delta r \\ \Delta \phi \end{bmatrix} + \begin{bmatrix} 0 & \frac{Y_{\delta_r}}{U_0} \\ L_{\delta_a} & L_{\delta_r} \\ N_{\delta_a} & N_{\delta_r} \\ 0 & 0 \end{bmatrix} \begin{bmatrix} \delta_a \\ \delta_r \end{bmatrix} \quad (13)$$

Lateral state-space matrices are calculated as follows

$$A_{\text{lat}} = \begin{bmatrix} -0.3478 & -0.001225 & -0.9673 & 0.6537 \\ -4.366 & -18.85 & 1.736 & 0 \\ 27.09 & -0.623 & -2.752 & 0 \\ 0 & 1 & 0 & 0 \end{bmatrix} \quad B_{\text{lat}} = \begin{bmatrix} 0 & 0.2609 \\ 136.6 & 1.198 \\ -3.971 & -22.37 \\ 0 & 0 \end{bmatrix}$$

$$C_{\text{lat}} = \begin{bmatrix} 1 & 0 & 0 & 0 \\ 0 & 1 & 0 & 0 \\ 0 & 0 & 1 & 0 \\ 0 & 0 & 0 & 1 \end{bmatrix} \quad D_{\text{lat}} = \begin{bmatrix} 0 & 0 \\ 0 & 0 \\ 0 & 0 \\ 0 & 0 \end{bmatrix}$$

The resulting 4th order lateral-directional linear model would be suitable for a control design where the goal is to regulate the UAV roll and yaw rates, as well as the angle of sideslip. Characteristic equation of the lateral-directional motion of the aircraft is composed of two distinct real roots and a pair of complex conjugate roots. These roots represent the lateral dynamics of the aircraft. Lateral modes are consisting of a slowly converged or diverged motion (spiral mode), a highly converged motion (roll mode), a lightly damped oscillatory motion with a low frequency (Dutch roll mode), respectively [McLean 1990].

Spiral mode

Spiral mode, which is a first order response and involves a relatively slow roll and yaw motion, may be stable or unstable concerning the aerodynamic specifications of the UAV. The main variables existing in the spiral motion are ϕ , ψ . β remains close to zero. A high degree of lateral stability C_{l_β} keeps the spiral motion in a stable region, whereas with a high degree of directional stability C_{n_β} , the spiral motion tends to instability.

Roll mode

The roll mode, which is a first order response that involves almost pure rolling motion about the x -stability axis, has a real root on the left-hand side. The roll motion is usually stable at low and moderate angles of attack, but it can lose its stability at high angles of attack. The roll mode is stimulated by an atmospheric disturbance or an aileron input. When a step aileron input is applied to the UAV, an exponential rise in roll rate is emerged until a steady state value is achieved. The roll damping stability coefficient C_{l_p} lead to control the value of the roll rate and roll mode time constant and is inversely proportional with these parameters. The magnitude of the roll damping L_p is a function of the size of the wing and tail surfaces.

Dutch roll mode

The Dutch roll mode is a second order response characterised by oscillations in the three lateral-directional motion variables β, ϕ, ψ , respectively. The Dutch roll mode generally starts with a sideslip perturbation followed by oscillations in roll and yaw angles. As the magnitude of C_{l_β} increases, roll coupling is, observed during the Dutch roll oscillations.

3. Robust H_∞ controller design for the UAV

3.1 Robust longitudinal attitude control system design

The primary control objective is to design a closed-loop system with desirable pilot handling qualities that are robust to time delay and modelling uncertainty. Increased damping is the oscillatory modes required for satisfactory handling performance. Time domain performance specifications such as rise times must also meet pilot expectations. Gain and phase margins must satisfy a specific value to ensure robustness. H_∞ optimization is posed as a model-matching problem utilizing an ideal tracking model to shape the pitch attitude response. Fig.2 shows H_∞ synthesis interconnection for the longitudinal controller in SIMULINK. Actuator dynamics and first order Pade approximation of the time delay are included in the plant.

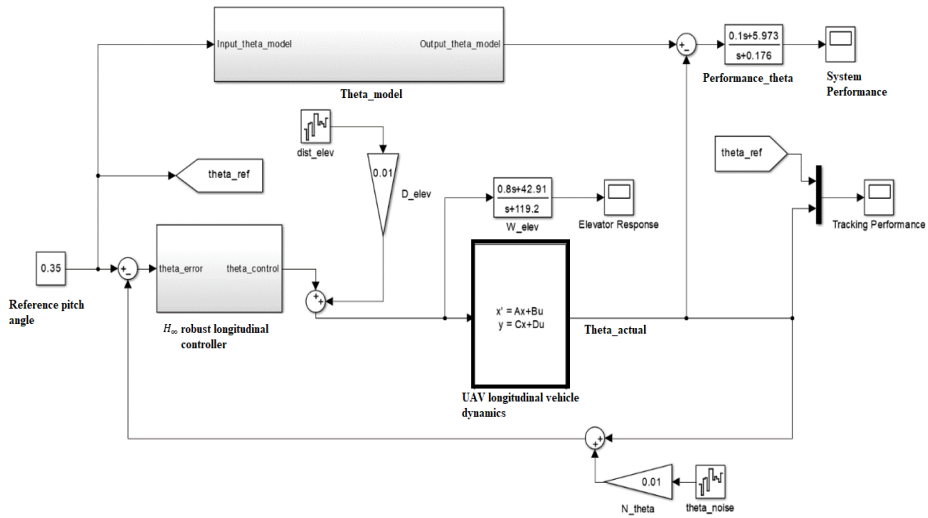


Fig. 2 H_{∞} pitch controller synthesis interconnection for pitch attitude case

Table 4 Weighting functions used to synthesise the longitudinal H_{∞} controller

Weight	Value
$Model_{\theta}$	$\frac{502.72(-s + 64.52)}{(s^2 + 5.6s + 16)(s + 31.42)(s + 64.52)}$
$Perf_{\theta}$	$\frac{0.1s + 5.973}{s + 0.176}$
D_{elev}	0.01
W_{elev}	$\frac{0.8s + 42.91}{s + 119.2}$
N_{θ}	0.01

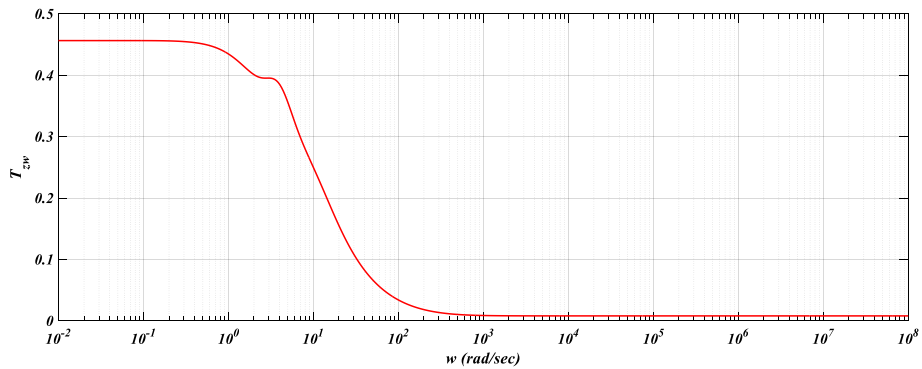


Fig. 3 The frequency response of the closed-loop system for pitch attitude control case

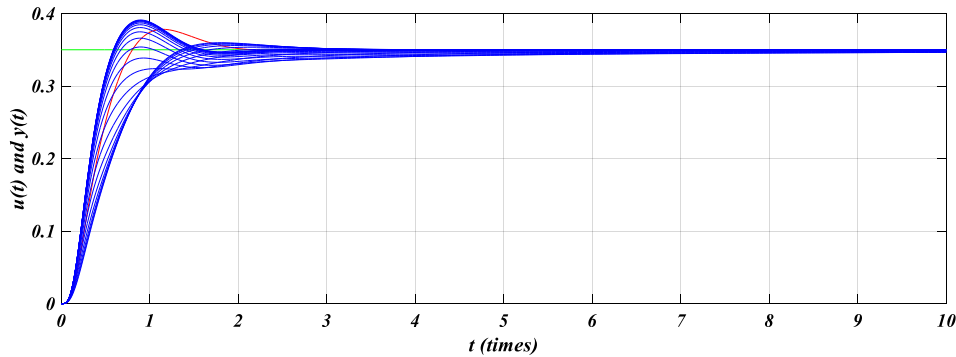
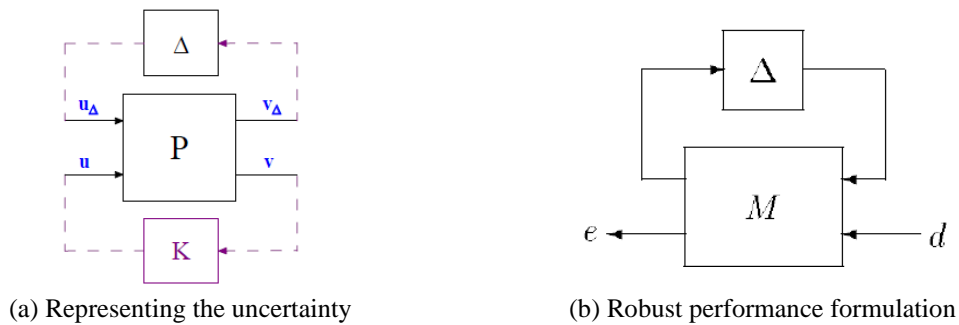


Fig. 4 Nominal and perturbed closed-loop system step responses for pitch attitude control case



(a) Representing the uncertainty (b) Robust performance formulation

Fig. 5 Robust performance scheme of an uncertain system

Ideal models and weighting function are used by the H_∞ framework to synthesize a controller. The desired input-output response is represented by an ideal tracking model. The bandwidth of the tracking model is set to achieve a desirable rise time in the closed-loop response. The ideal model is also augmented with actuator dynamics and a linear approximation of the time delay to improve controller performance. A frequency dependent performance weight is used to shape the closed-loop response to match the ideal system. Additional considerations include control effort penalty to avoid high gain in the controller and a measurement noise corruption to prevent plant inversion. Disturbance on the elevator is used to improve robustness. Table 4 summarizes the weighting functions used for the longitudinal H_∞ control synthesis optimization.

The $\mu(Mu)$ Toolbox in MATLAB was used to synthesise the H_∞ longitudinal controller. Gamma value achieved is 0,4564. The controller transfer function was found as given below

$$Ks_{pitch} = \frac{4.198 (s+119.2) (s+64.52) (s+31.44) (s+20) (s+2.509) (s^2 + 6.814s + 33.54) (s^2 + 29.56s + 309.5)}{(s+64.52)(s+53.42)(s+31.41)(s+26)(s+7.761)(s+2.01) (s^2 + 7.453s + 30.71) (s^2 + 26.52s + 352.6)}$$

The frequency response of the closed-loop control system is given in Fig. 3.

The response is flat and the H_∞ norm of the pitch attitude closed-loop system is $\|T_{zw}\|_\infty = 0.4564$. The system response was tested for several allowed perturbations. Nominal and perturbed system responses was shown in Fig 4.

These results demonstrate that the closed-loop damping is reduced. The general pitch angle tracking performance objective is satisfied under various perturbations. Robust performance formulation given in Fig. 5 was utilised to evaluate the amount of the system uncertainty.

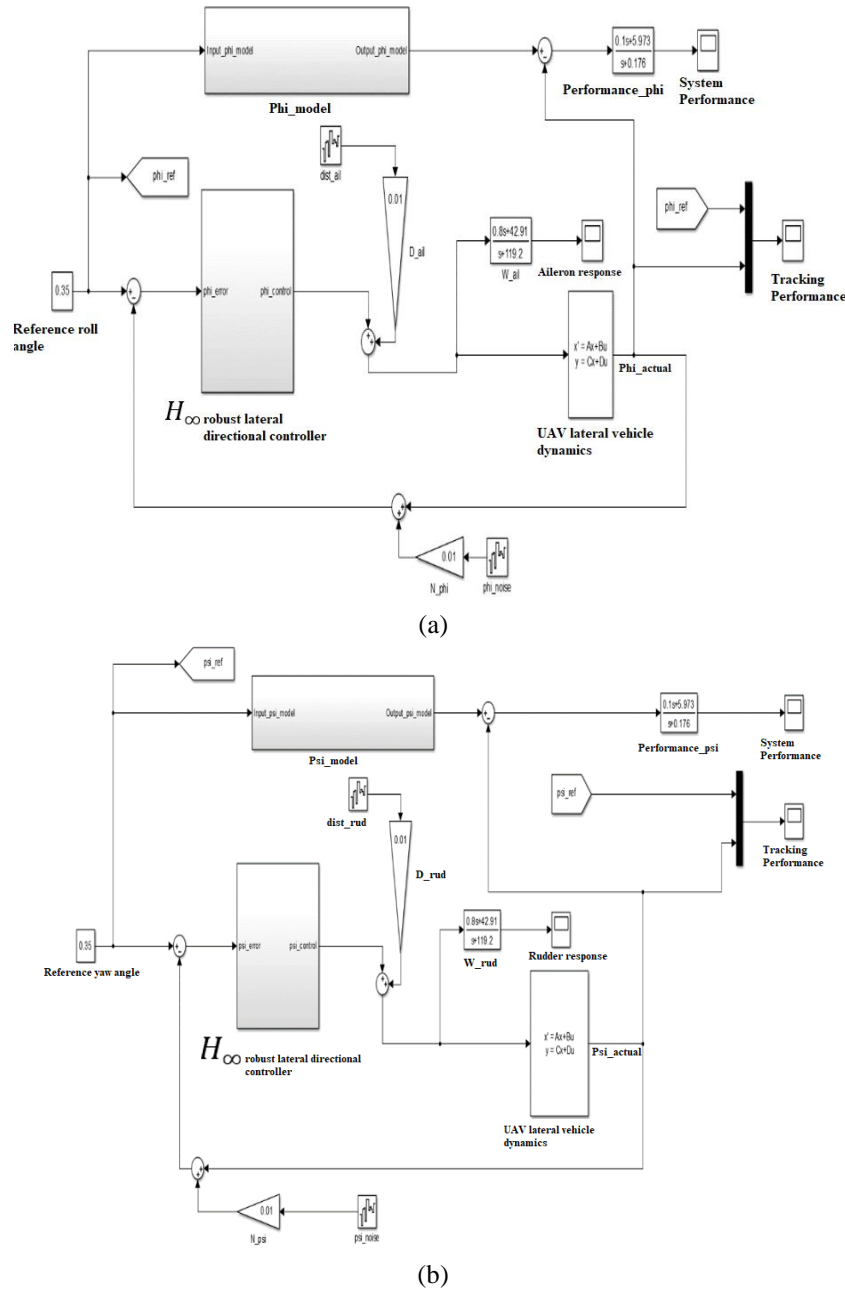


Fig. 6 H_{∞} lateral controller synthesis interconnection for (a) roll attitude case and (b) yaw attitude case

Δ is a structured perturbation from an allowable uncertainty set, M is the non-perturbed system model, P is the generalized plant, K is the robust controller, u and v are system input and system output, respectively, d and e are the generalized disturbance and error, which define the performance objective, respectively. Note that the uncertainty block Δ is assumed to be a diagonal-structured full complex matrix $\Delta \in C^{r \times p}$. It is possible to find robustness of a given

system by the help of the μ through the help of the following theorem:

Theorem: The loop given in Fig. 5(b) is well-posed and internally stable for all Δ with $\|\Delta\|_\infty \leq \beta$ if and only if $\sup_{\omega \in \mathcal{R}} (M(j\omega)) \leq \beta$ (J.C. Doyle, 1982a; J.C. Doyle and G.Stein, 1981, Doyle et al, 1982b)

3.2 Robust lateral attitude control system design

The lateral/directional dynamics of the UAV are governed by a very slow stable spiral mode, a fast lightly damped Dutch roll mode, and a slightly faster stable roll model. Actuator and time delay models as the same as they were for the longitudinal case. The design objectives for the lateral/directional controller are like those for the longitudinal controller. The closed-loop system must achieve satisfactory pilot handling performance and be robust for time delay and modelling uncertainty. For the lateral/directional closed loop system, damping is to be increased in the Dutch roll mode to reduce oscillations. An H_∞ model-matching problem is posed for the lateral/directional controller, and the interconnections are shown in Fig. 6(a) and Fig.6(b) for roll and yaw attitude, respectively.

Table 5 summarises the weighting functions used for the lateral/directional H_∞ control synthesis optimization.

The closed-loop lateral dynamics achieve higher damping in the Dutch roll mode but otherwise are like the open-loop response. The Mu-Toolbox in MATLAB [Dorobantu *et al.* 2012, Logan 1994] was used to synthesise the H_∞ lateral controller. Gamma value achieved is 1.1261 and 2.3762 for the roll and yaw attitudes, respectively. The controller transfer function was found for the roll and yaw attitudes as follows

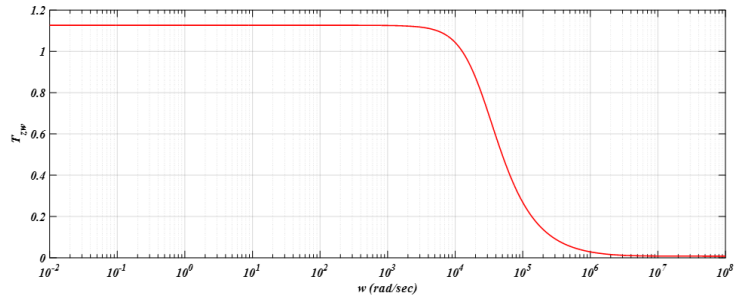
$$Ks_{roll} = \frac{34552.5671 (s+119.2) (s+20) (s+18.81) (s+3.31) (s^2 + 0.9859s + 10.41) (s^2 + 3.186s + 27.74)(s^2 + 6.353s+2381)}{(s^2 + 2.455 \cdot 10^4) (s+2.523)(s^2 + 3.043s+26.97)(s^2 + 0.2646s+39)(s^2 + 49.94s+1042)(s^2 + 6.353s+2381)}$$

$$Ks_{yaw} = \frac{2628018.5334 (s + 119.2) (s + 20) (s + 18.81) (s + 1.756)(s + 0.1344) (s^2 + 2.974s + 7.262) (s^2 + 3.186s + 27.74)(s^2 + 6.353s + 2381)}{(s + 8.848 \cdot 10^5) (s + 53.52)(s + 25.37)(s + 0.9963)(s^2 + 2.721s + 7.448)(s^2 + 3.097s + 27.24)(s^2 + 21.13s + 159.9)(s^2 + 6.353s + 2381)}$$

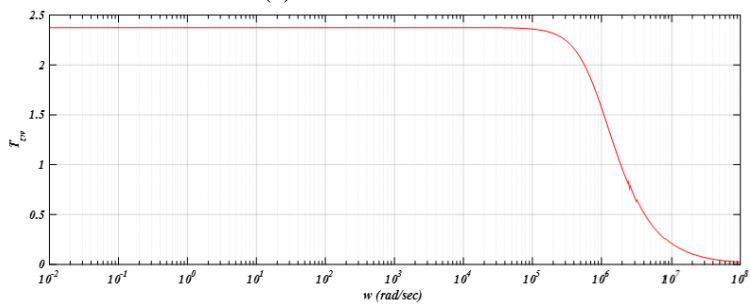
The frequency response of the closed-loop system is given in Fig. 7 (a) and Fig.7 (b) for roll and yaw attitude case, respectively.

Table 5 Weighting functions used to synthesise the lateral/directional H_∞ controller

Weight	Value
$Model_{\phi/\psi}$	$\frac{244.44(-s + 64.52)}{(s^2 + 3.92s + 7.78)(s + 31.42)(s + 64.52)}$
$Perf_{\phi/\psi}$	$\frac{0.1s + 5.973}{s + 0.176}$
$D_{ail/rudder}$	0.01
$W_{ail/rudder}$	$\frac{0.8s + 42.91}{s + 119.2}$
$N_{\phi/\psi}$	0.01

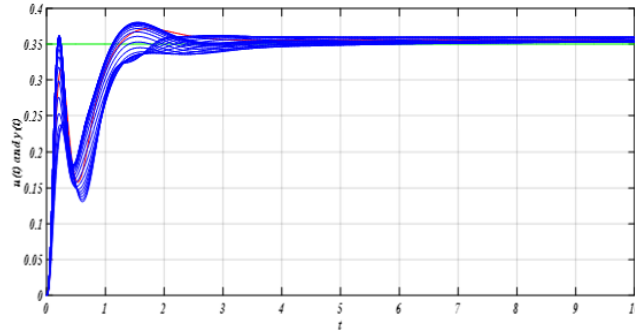


(a) Roll attitude case

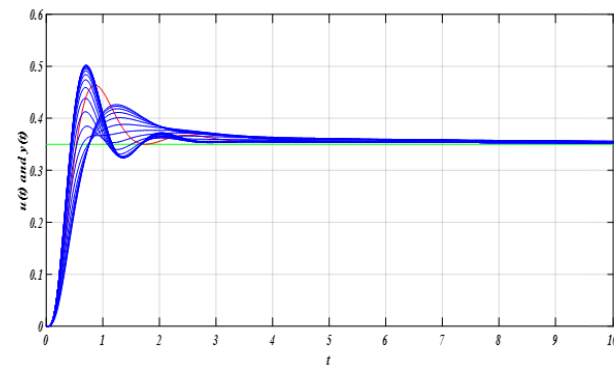


(b) Yaw attitude case

Fig. 7 The frequency response of the closed-loop system



(a) Roll attitude case



(b) Yaw attitude case

Fig. 8 Nominal and perturbed system responses

The responses are flat and the H_∞ norm of the roll and yaw attitude closed-loop system are $\|T_{zw}\|_\infty = 1.1261$, $\|T_{zw}\|_\infty = 2.3762$, respectively.

The system response was tested for several allowed perturbations. Nominal and perturbed system responses were shown in Fig. 8 (a) and Fig.8 (b) for roll and yaw attitude case, respectively.

In conclusion, the roll and yaw angle tracking and lateral performance are satisfied.

4. Conclusions

In this paper, the general procedure of modelling a UAV and robust autopilot design was presented. Evaluating the stability and control coefficients, which define the characteristics of the dynamical behaviours of the UAV, is essential for designing a high-performance autopilot.

When system parameters are uncertain, or UAV is subjected to exogenous disturbance, the performance of the autopilots deteriorate. For this reason, the advantage of the non-adaptive or non-robust displacement autopilots, whose controllers have fixed gains on the feedback path, disappears. Therefore, the performance and robustness evaluation, which would greatly benefit as compared to equivalent properties of a baseline controller, was sought by designing a robust H_∞ control framework utilized to synthesize a multivariable control architecture. Design objectives comprise robustness w.r.t sensor noise and exogenous disturbance. Moreover, the satisfactory pilot handling performance criterion for improving the reliability of flight control systems subjected to adverse conditions, such as faults or subsystem failures was developed. The robustness and stability of the pitch, roll and yaw autopilot was assured through proposed architecture. It can be inferred that a robust control strategy has the potential to improve a pilot's ability to maneuver in the presence of disturbance, sensor noise and model uncertainty.

References

- Abuhashim, T. and Sukkarieh, S. (2012), "Incorporating geometric information into Gaussian Process terrain models from monocular images", *Proceedings of the IEEE/RSJ International Conference on Intelligent Robots and Systems*, Vilamoura, Algarve, Portugal, October.
- Åström, K.J. and Wittenmark, B. (2009), *Adaptive Control*, Pearson Education.
- Blakelock, J.H. (1991), *Automatic Control of Aircraft and Missiles*, John Wiley & Sons, New York, U.S.A.
- Butler, H. (1992), *Model Reference Adaptive Control: From Theory to Practice*, Prentice Hall, Upper Saddle River, New Jersey, U.S.A.
- Chang, K. (2003), "A modified robust adaptive control with dead zone for nonlinear plants with bounded disturbance", *Syst. Anal. Model. Simul.*, **43**(1), 27-38. <https://doi.org/10.1080/02329290290001065>.
- Dorobantu, A., Murch, A. and Balas, G. (2012), "H-infinity robust control design for the NASA AirSTAR flight test vehicle", *Proceedings of the 50th AIAA Aerospace Sciences Meeting including the New Horizons Forum and Aerospace Exposition*, Nashville, Tennessee, U.S.A., January.
- Du, Y. (2011), "Development of real-time flight control system for the low-cost vehicle", M.Sc. Dissertation, Cranfield University, Bedfordshire, U.K.
- Giacomán-Zarzar, M., Ramirez-Mendoza, R., Fleming, P., Griffin, I. and Molina-Cristóbal, A. (2008), "Robust H_∞ controller design for aircraft lateral dynamics using multi-objective optimization and genetic algorithm", *IFAC Proc. Vol.*, **41**(2), 8834-8839. <https://doi.org/10.3182/20080706-5-KR-1001.01493>.
- Guo, J., Tao, G. and Liu, Y. (2011), "A multivariable MRAC scheme with application to a nonlinear aircraft model", *Automatica*, **47**(4), 804-812. <https://doi.org/10.1016/j.automatica.2011.01.069>.
- Hassan, H. and Rao, M. (2005), "Novel e-modification robust adaptive control scheme using non-quadratic

- Lyapunov functions for higher order systems”, *Proceedings of the EUROCON 2005- The International Conference on Computer as a Tool*, Belgrade, Serbia, November.
- Ioannou, P.A. and Sun, J. (1996), *Robust Adaptive Control*, Prentice Hall, Upper Saddle River, New Jersey, U.S.A.
- Ioannou, P. and Datta, A. (2006), *Robust Adaptive Control: Design, Analysis and Robustness Bounds*, in *Foundations of Adaptive Control Lecture Notes in Control and Information Sciences*, Springer, Berlin, Heidelberg, Germany. 71-152.
- Ioannou, P. and Kokotovic, P. (1984), “Instability analysis and improvement of robustness of adaptive control”, *Automatica*, **20**(5), 583-594. [https://doi.org/10.1016/0005-1098\(84\)90009-8](https://doi.org/10.1016/0005-1098(84)90009-8).
- Ioannou, P. and Sun, J. (1991), “Robust adaptive control: A unified approach”, *Proceedings of the 28th IEEE Conference on Decision and Control*, Tampa, Florida, U.S.A., December.
- Doyle, J. and Stein, G. (1981) “Multivariable feedback design: Concepts for a classical/modern synthesis”, *IEEE T. Autom. Control*, **26**(1), 4-16. <https://doi.org/10.1109/TAC.1981.1102555>.
- Doyle, J. (1982a), “Analysis of feedback systems with structured uncertainties”, *IEE Proc D-Control Theor. Appl.*, **129**(6), 242-250. <https://doi.org/10.1049/ip-d.1982.0053>.
- Doyle, J.C., Wall, J.E. and Stein, G. (1982b), “Performance and robustness analysis for structured uncertainty”, *Proceedings of the 21st IEEE Conference on Decision and Control*, Orlando, Florida, U.S.A., September.
- Khalil, H.K. (2015), *Nonlinear Systems*, Pearson Education International, Noida, India.
- Lavretsky, E. (2014), *Robust and Adaptive Control Methods for Aerial Vehicles*, in *Handbook of Unmanned Aerial Vehicles*, 675-710.
- Lavretsky, E. and Wise, K.A. (2013), *Robust and Adaptive Control with Aerospace Applications*, Springer, London, U.K.
- Logan, C. (1994), “A comparison between H-infinity/Mu-synthesis control and sliding-mode control for robust control of a small autonomous underwater vehicle”, *Proceedings of the IEEE Symposium on Autonomous Underwater Vehicle Technology (AUV94)*, Cambridge, Massachusetts, U.S.A.
- McLean, D. (1990), *Automatic Flight Control Systems*, Prentice Hall, New York, U.S.A.
- Mystkowski, A. (2013), “Robust Optimal Control of MAV Based on Linear-Time Varying Decoupled Model Dynamics”, *Solid State Phenom.*, **198**, 571-576. <https://doi.org/10.4028/www.scientific.net/SSP.198.571>.
- Mystkowski, A. (2014), “Implementation and investigation of a robust control algorithm for an unmanned micro-aerial vehicle”, *Robot. Autonom. Syst.*, **62**(8), 1187-1196. <https://doi.org/10.1016/j.robot.2014.04.002>.
- Narendra, K., Lin, Y. and Valavani, L. (1980), “Stable adaptive controller design, part II: Proof of stability”, *IEEE T. Autom. Control*, **25**(3), 440-448. <https://doi.org/10.1109/TAC.1980.1102362>.
- Nelson, R.C. (1998), *Flight stability and Automatic Control*, McGraw-Hill, Boston, Massachusetts, u.S.A.
- Tao, G. (2003), *Adaptive Control Design and Analysis*, John Wiley & Sons Inc., U.S.A.
- Tao, G. and Joshi, S. M. (2001), *Adaptive Control of Systems with Actuator Failures*, in *Adaptive Control of Nonsmooth Dynamic Systems*, Springer Science & Business Media., 111-156.
- Valavanis, K.P. (2015), *Handbook of Unmanned Aerial Vehicles*, Springer, Dordrecht, The Netherlands.
- Wang, Q., Hou, Y. and Dong, C. (2011), “Model reference robust adaptive control for a class of uncertain switched linear systems”, *Int. J. Robust Nonlin. Control*, **22**(9), 1019-1035. <https://doi.org/10.1002/rnc.1744>.

CC

Nomenclature

\underline{x} State vector

\underline{y}	Output signal
\underline{u}	Control signal.
I_x, I_y, I_z	Moments of inertia about the roll, pitch and yaw axis, respectively
I_{yz}, I_{xz}, I_{xy}	Products of inertia about the roll, pitch and yaw axis, respectively
m	Total mass of the UAV
p, q, r	Body angular rates at roll, pitch and yaw axis, respectively
u, v, w	Body linear velocity components at the roll, pitch and yaw axis, respectively
F_{Ax}, F_{Ay}, F_{Az}	Aerodynamic force components at the roll, pitch and yaw axis, respectively
F_{Tx}, F_{Ty}, F_{Tz}	Thrust force components at the roll, pitch and yaw axis, respectively
F_{Gx}, F_{Gy}, F_{Gz}	Gravitational force components at the roll, pitch and yaw axis, respectively
L, D, T	Lift, drag, thrust forces, respectively
g	Acceleration due to gravity
ϕ, θ, ψ	Roll, pitch and yaw Euler angles, respectively
α	Angle of attack
ϕ_T	Thrust angle
L_A, M_A, N_A	Aerodynamic moment components at the roll, pitch and yaw axis, respectively
L_T, M_T, N_T	Thrust moment components at the roll, pitch and yaw axis, respectively
Q	Flight dynamic pressure
S	Wing platform area
C_D	Drag coefficient
$C_{D\alpha}$	Derivative of the drag coefficient w.r.t angle of attack
$C_{D\delta_e}$	Derivative of the drag coefficient w.r.t elevator deflection
C_{Dq}	Derivative of the drag coefficient w.r.t pitch angular rate
$\delta_a, \delta_e, \delta_r$	Aileron, elevator and rudder deflection, respectively

C_L	Lift coefficient
$C_{L\alpha}$	Derivative of the lift coefficient w.r.t angle of attack
$C_{L\dot{\alpha}}$	Derivative of the lift coefficient w.r.t rate of the angle of attack
$C_{L\delta_e}$	Derivative of the lift coefficient w.r.t elevator deflection
C_{Lq}	Derivative of the lift coefficient w.r.t pitch angular rate
c	Characteristic length for longitudinal dynamic
b	Characteristic length for lateral dynamic
U_0	Forward velocity of the UAV
β	Sideslip angle
C_y	Side force coefficient
$C_{y\beta}$	Derivative of the side force coefficient w.r.t sideslip angle
$C_{y\dot{\beta}}$	Derivative of the side force coefficient w.r.t rate of the sideslip angle
$C_{y\delta_a}$	Derivative of the side force coefficient w.r.t aileron deflection
$C_{y\delta_r}$	Derivative of the side force coefficient w.r.t rudder deflection
C_{yp}	Derivative of the side force coefficient w.r.t roll angular rate
C_{yr}	Derivative of the side force coefficient w.r.t yaw angular rate
C_l	Rolling moment coefficient
$C_{l\beta}$	Derivative of the rolling moment coefficient w.r.t sideslip angle
$C_{l\delta_a}$	Derivative of the rolling moment coefficient w.r.t aileron deflection
$C_{l\delta_r}$	Derivative of the rolling moment coefficient w.r.t rudder deflection
C_{lp}	Derivative of the rolling moment coefficient w.r.t roll angular rate
C_{lr}	Derivative of the rolling moment coefficient w.r.t yaw angular rate
C_m	Pitching moment coefficient

C_{m_α}	Derivative of the pitching moment coefficient w.r.t angle of attack
$C_{m_{\delta_e}}$	Derivative of the pitching moment coefficient w.r.t elevator deflection
$C_{m_{\dot{\alpha}}}$	Derivative of the pitching moment coefficient w.r.t rate of the angle of attack
C_{m_q}	Derivative of the pitching moment coefficient w.r.t pitch angular rate
C_n	Yawing moment coefficient
C_{n_β}	Derivative of the yawing moment coefficient w.r.t sideslip angle
$C_{n_{\dot{\beta}}}$	Derivative of the yawing moment coefficient w.r.t rate of sideslip angle
$C_{n_{\dot{\alpha}}}$	Derivative of the yawing moment coefficient w.r.t rate of the angle of attack
C_{n_α}	Derivative of the yawing moment coefficient w.r.t angle of attack
$C_{n_{\delta_r}}$	Derivative of the yawing moment coefficient w.r.t rudder deflection
$C_{n_{\delta_a}}$	Derivative of the yawing moment coefficient w.r.t aileron deflection
C_{n_p}	Derivative of the yawing moment coefficient w.r.t roll angular rate
C_{n_r}	Derivative of the yawing moment coefficient w.r.t yaw angular rate
δ_T	Throttle setting
z_T	Distance from the thrust motor to the center of gravity in the z-direction
h	Flight altitude
ρ	Air density